Spacial Distribution of Photoneutrons in an Iron Slab Produced by 20-MeV Electron Bombardment

By

Takashi NAKAMURA*, Hideo HIRAYAMA**, Seiji NISHINO*
and Tomonori HYODO*

(Received September 29, 1973)

Abstract

Photoneutron distribution was measured with activation of aluminum and magnesium in an iron slab bombarded by a beam of 20-MeV electrons from a linear accelerator. In order to compare with the experimental results, the spacial neutron distribution was calculated as follows: the photoneutron source distribution originating from the photonuclear reaction was calculated by an approximate analytical method; and the neutron distribution in the medium was calculated on the basis of this distributed source by Monte Carlo code, CYGNUS. The calculated neutron distribution was in good agreement with the measured distribution, using activities of aluminum detectors. From the comparison of both saturated activities of aluminum and magnesium, it is found that the photonuclear effects are remarkable when r is equal to 10 cm and Z is between 2 and 5 cm.

The spacial distribution of neutron flux above about 6.5 MeV in the iron slab is nearly spherical symmetric around the beam incident point; and an exponential attenuation with the slope of effective removal cross section of iron, $\Sigma_{eff}{}^{R}=0.172\ \mathrm{cm}^{-1}$.

I. Introduction

Various kinds of high energy accelerators have recently been in practical use in many fields, not to speak of nuclear physics. It is a very important problem to protect mankind and instruments from a large amount of radiation, especially bremsstrahlung and photoneutrons, generating from a target bombarded by accelerating particles.

The photoneutron target has been frequently used as a fission neutron source based upon the similarlity between their spectra. Many precise measurements of

* Department of Nuclear Engineering.
** Department of Nuclear Engineering. Present address: National Laboratory for High Energy Physics.

neutron spectra have been performed by use of the time-of-flight method. However, by this method it is difficult to know the special distribution of neutrons in the target medium. The spacial distribution of photoneutrons in the medium generated by the charged particle bombardment had been measured by threshold detectors[1], but there has been no systematic study for the spacial distribution of photoneutrons caused by electron-induced bremsstrahlung. This may be because flux of bremsstrahlung is dominant in comparison with photoneutron flux, so the effect of photonuclear reaction in threshold detectors cannot be neglected[2,3].

To calculate the photoneutron spectrum, it is necessary to pursue the cascade phenomenon precisely from electron incidence to neutron emission and attenuation. The electron-photon cascade has been investigated by the Monte Carlo method[4~6] and the approximate numerical calculation[7~9], while the neutron transport has been calculated by the Monte Carlo method[10,11] and the numerical solution of transport equation[12~16]. There has been no theoretical study to combine both of them, excluding the simple analytical calculation to obtain the neutron yield of the target[17~19].

In this study, an iron slab was bombarded by a 20-MeV electron beam from the linear accelerator of the Research Reactor Institute of Kyoto University, and the photoneutron distribution in the slab was measured with threshold detectors. The calculation of the photoneutron distribution was carried out as follows: the neutron source distribution originating from the photonuclear reaction was calculated by an approximate analytical method[9]; and the neutron distribution in the medium was calculated by the Monte Carlo code, CYGNUS[11]. The calculated neutron distribution was compared with the saturated activities of threshold detectors in the medium.

II. Experimental

The experiments were performed using a 20-MeV electron linear accelerator of the Research Reactor Institute of Kyoto University. The external appearance of the experimental arrangement is illustrated in Photo. 1. The 20-MeV electrons struck the iron slab of 18.5 cm in thickness by 80×60 cm^2 in area faced perpendicularly to the beam axis. The photoneutron distribution in the slab was measured by the activation detectors of aluminum and magnesium. The experimental result of the aluminum detector indicated a neutron flux due only to the $^{27}Al(n, \alpha)^{24}Na$ reaction, while that of the magnesium detector includes to some extent a photon flux due to the $^{25}Mg(\gamma, p)^{24}Na$ reaction, in addition to a neutron flux due to the $^{24}Mg(n, p)^{24}Na$ reaction. The cross section shape of the $^{24}Mg(n, p)^{24}Na$ reaction is almost the same as that of the $^{27}Al(n, \alpha)^{24}Na$ reaction from the threshold energy to 8.5 MeV, so the effect of photoproton is examined by a comparison of both saturated activities. The

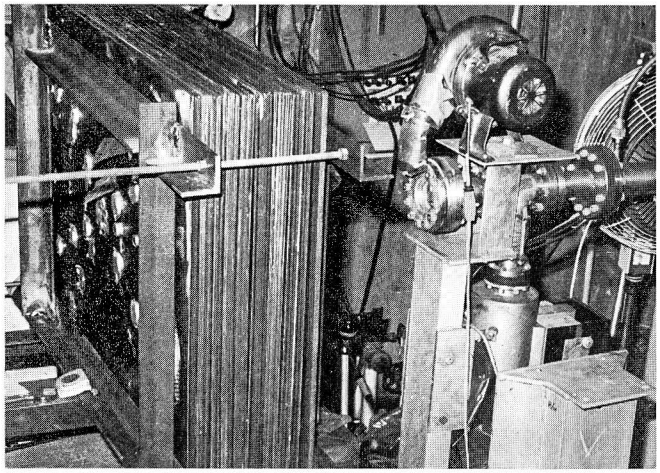

Photo. 1. External appearance of the experimental arrangement.

Table 1 Sizes and physical properties of activation detectors

Element	Abundance (%)	Reaction	Radius (cm)	Thickness (cm)	γ-ray Energy (MeV)
^{27}Al	100	^{27}Al$(n, \alpha)^{24}$Na	1.5	0.6	1.37 2.754
			1.0	0.0015	1.37 2.754
^{24}Mg	78.6	^{24}Mg$(n, p)^{24}$Na	1.5	0.6	1.37 2.754
^{25}Mg	10.1	^{25}Mg$(\gamma, p)^{24}$Na	1.5	0.6	1.37 2.754

size and physical properties of these detectors are shown in Table 1. Detectors were fixed with Scotch tape at the following (r, z)-positions in the slab, where r is the lateral distance from the electron beam axis and z the longitudinal distance from the front face of the iron slab, $r=2$, 10, 20, 30 cm and $t=0$, 1.9, 4.9, 9.7 and 18.5 cm, respectively.

The gamma-ray activities of the detectors induced by photoneutrons were detected by a 3-in.-diam. by 3-in.-long NaI(Tl) scintillator coupled to a multi-channel pulse height analyzer. The saturated activities are obtained by the following equation,

$$A_i = \frac{\lambda_i C_p{}^i}{N_T{}^i \eta_i \varepsilon_p{}^i e^{-\lambda_i T_w}(1-e^{-\lambda_i T_{ir}})(1-e^{-\lambda_i T_c})}, \qquad (1)$$

where λ_i is the decay constant of the i-th isotope, η_i the photon number per decay of the i-th isotope, $N_T{}^i$ the total number of nuclei of the i-th isotope in the detector, $C_p{}^i$

the peak counting rate, ε_p^t the peak efficiency of the detector, T_w the waiting time, T_{ir} the irradiation time and T_c the counting time. The peak efficiency ε_p^t of NaI(Tl) scintillator was calculated with the Monte Carlo code, REFUM[20].

III. Method of Calculation

1. Approximate Calculation of Neutron Source Distribution

The spacial distribution of neutron source due to the photonuclear reaction in the iron scatterer was obtained from multiplying the Fe(γ, n) cross section, $\Sigma_{\gamma n}(K)$, by the spacial energy distribution of bremsstrahlung of energy K at the (r, z)-position, $\psi_\gamma(K, r, z)$, calculated numerically with a simple analytical approximation[7~9]. The iron slab has been subdivided into a number of n thin slabs, each with a thickness Δt. Within each thin slab the electron will travel in a direction defined by the polar angle, θ, and azimuthal angle, ϕ, emitting a photon in the direction of angle ω. Under the rough approximation of the electron continuous by slowing-down model and neglecting the electron lateral displacement, the bremsstrahlung spectrum generated at the (r, z)-position is given by

$$\psi_\gamma(K, r, z) = \sum_{i=1}^{n} \int_0^{2\pi} d\varphi_i \int_0^{\pi} \sin\theta_i d\theta_i \tau(E_0, t_i)\nu_i \times F(E_i, \theta_i, t_i)\frac{d^2\sigma}{dKd\Omega}(E_i, K, w_i)\, Y_i(K, r, z)d\Omega \qquad (2)$$

$$(E_i \geq K),$$

where E_0 is the incident electron energy, E_i the average electron energy in the i-th thin slab, t_i the average depth of the i-th thin slab, τ the electron transmission factor which neglects the δ-ray production on Ebert's formula[21], F the electron angular distribution by Bethe[22] and Frank[23], and finally ν_i the number of atoms per unit cross section in the i-th thin slab*. In this calculation, the electron-photon cascade and the backward emission of bremsstrahlung were neglected; and the scattering of photons was considered only as a term of the buildup factor. The result of the calculation is shown in Fig. 1.

The number of photoneutrons generated at the (r, z)-position, $s(E_n, r, z)$ is given by

$$s(E_n, r, z) = \psi_\gamma(K, r, z)\Sigma_{\gamma n}(K), \qquad (E_n = K - E_B), \qquad (3)$$

where $\Sigma_{\gamma n}(K)$ is the macroscopic (γ, n) cross section[24], E_n the neutron energy and

* See Eq. (5) in Ref. (9).

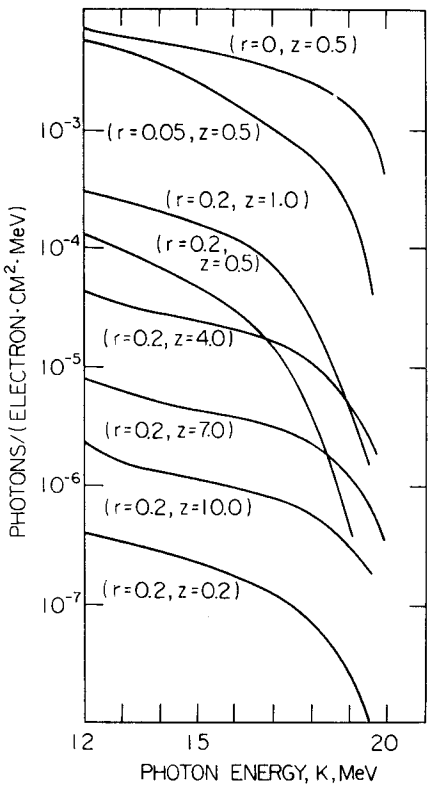

Fig. 1. Calculated bremsstrahlung energy spectra at some (r, z)-positions in the iron slab, where r is the lateral distance from the electron beam axis and z the longitudinal distance from the front face of the iron slab.

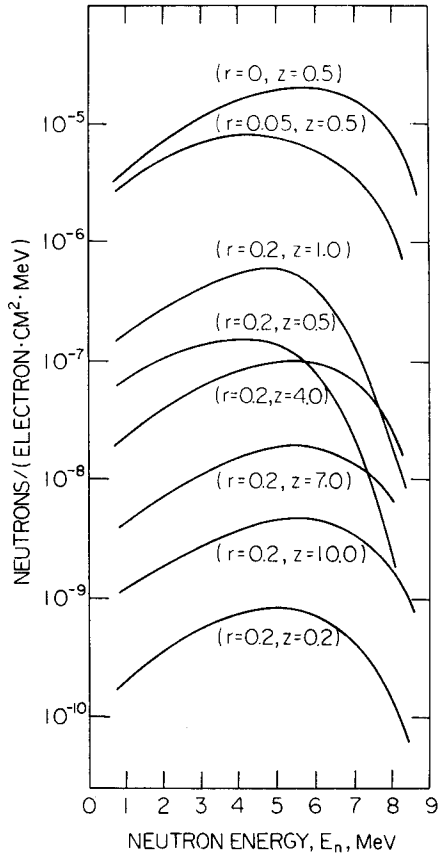

Fig. 2. Calculated photoneutron-source energy spectra at some (r, z)-positions in the iron slab.

E_B the neutron binding energy of iron nuclei. The calculated photoneutron spectra, $s(E_n, r, z)$ at some (r, z)-positions in the iron scatterer are shown in Fig. 2. The spacial distribution of photoneutron source in the scatterer $S(r, z)$

$$S(r, z) = \sum_{E_n} s(E_n, r, z), \tag{4}$$

is shown in Fig. 3. This figure clearly indicates that a large percentage of photoneutron generates in the nearest neighbourhood of the electron incident point and its amount decreases sharply with increasing r and z.

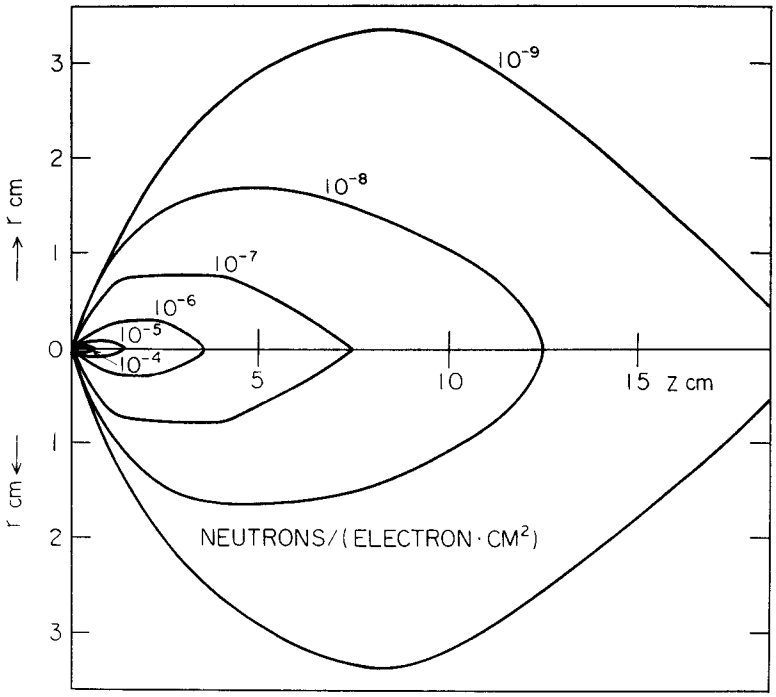

Fig. 3. Spacial distribution of the photoneutron source as a function of r and z.

The neutron distribution in the iron slab was calculated with the Monte Carlo code, CYGNUS[11], using the source distribution $S(r, z)$, described above.

The neutron path was traced in succession to the decision of the position, direction and energy of the primary neutron. The neutron energy spectrum at the (r, z)-position in the iron slab, $\psi_n(E_n, r, z)$ was obtained by summations over the sample collision density from each scattering point in the medium as follows:

$$\psi_n(E_{nl}, r_j, z_k) = \frac{1}{I}\sum_{i=1}^{I}\sum_{m=0}^{L_j} B_m{}^j(i)P_m(i)Q_m{}^j(i)f_m{}^{lk}(i). \tag{5}$$

The boundary condition, $B_m{}^j(i)$ is unity when the neutron crosses the cylindrical face of $r=r_j$ and zero otherwise. The factor

$$P_m(i) = \prod_{m=0}^{m-1} \exp[-\Sigma_a\{E_{nn}(i)\}\cdot l_{n+1}(i)], \tag{6}$$

is the probability that the neutron has not been absorbed in the i-th history prior to the state immediately after its m-th scattering, where Σ_a is the macroscopic absorption

cross section and $l_{n+1}(i)$ is the free path from the n-th scattering point to the $(n+1)$-th scattering point in the i-th history. The quantity $Q_m{}^j(i)$ denoted the probability that a neutron will reach the face $r=r_j$ without further collision from the m-th scattering point in the i-th history,

$$Q_m{}^j(i) = \exp[-\Sigma_t\{E_{nm}(i)\} \cdot t_m{}^j(i)], \tag{7}$$

where Σ_t is the macroscopic total cross section and $t_m{}^j(i)$ is the distance from the m-th scattering point to the face $r=r_j$ measured along the flight path after the m-th collision. The energy-longitudinal position classification factor $f_m{}^{lk}(i)$ is equal to

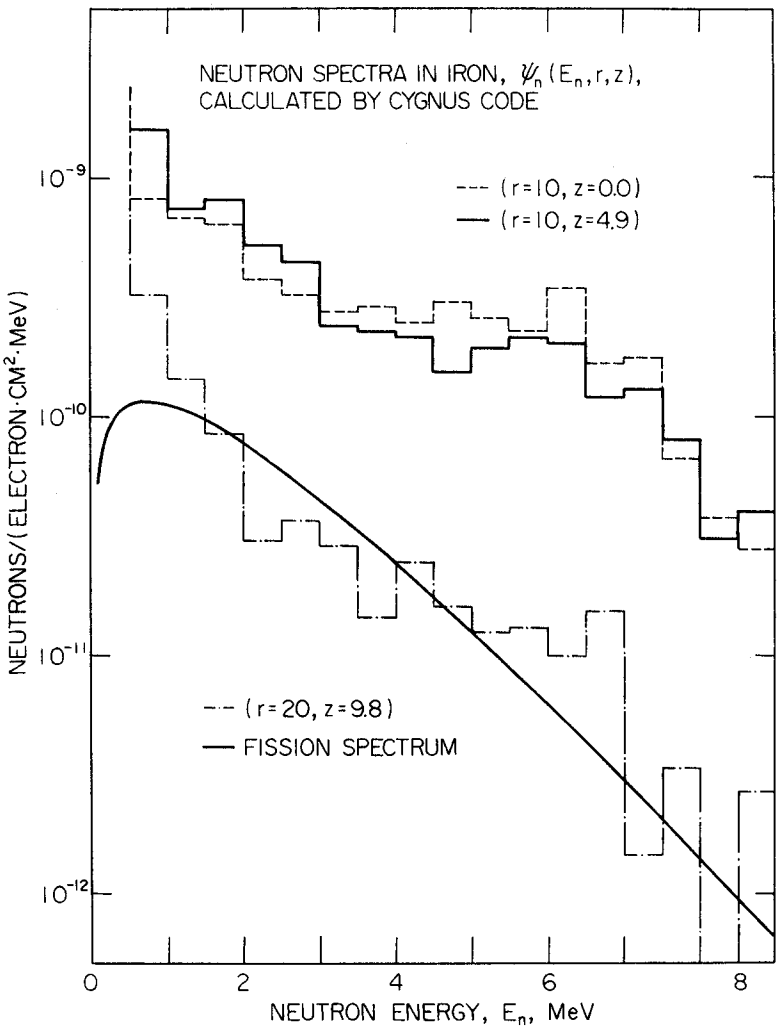

Fig. 4. Neutron energy spectra at some (r, z)-positions in the iron slab.

unity when E_n is in the l-th energy interval and z is in the k-th position interval, and zero otherwise.

Some examples of the neutron energy spectra calculated from Eq. (5) are shown in Fig. 4. The neutron spectra at the positions of $(r, z)=(10.0, 0.0)$ and $(r, z)=(10.0, 4.9)$ are harder than the fission spectrum, while that at the position of $(r, z)=(20.0, 9.7)$ is similar to the fission spectrum, in spite of the neutron source energy spectrum having a broad peak near 5 MeV, as shown in Fig. 3. This calculated result is consistent with the well known experimental fact that the neutron spectrum from the target is close to the fission spectrum.

IV. Comparison Between Experiment and Calculation

Fig. 5 shows the variation of the Al(n, α) activations per electron with the longi-

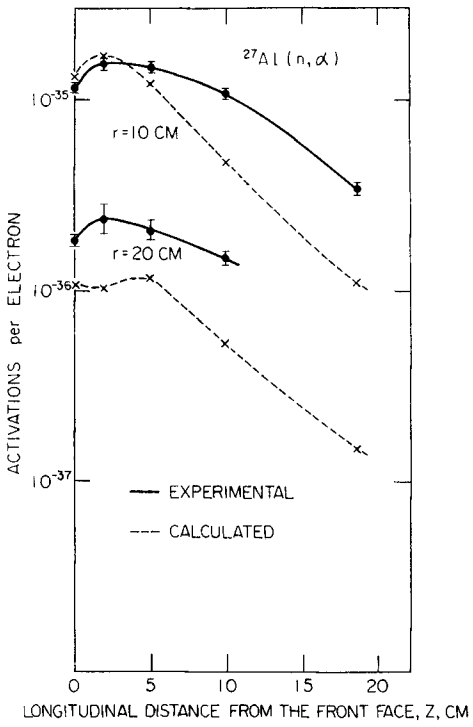

Fig. 5. Variation of the Al(n, α) activations with z for r=10 and 20 cm.

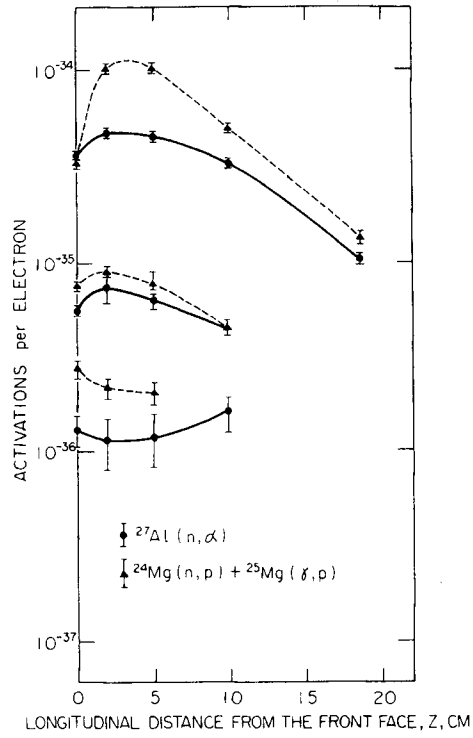

Fig. 6. Comparison of the variation of the activation of aluminum and magnesium with z for r=10, 20 and 30 cm. The aluminum results are multiplied by factor 3.3 which is the ratio of both cross section ^{24}Mg(n, p)^{24}Na and ^{27}Al(n, α)^{24}Na for 6.5 MeV neutron.

tudinal distance from the electron incident face, z, for 10 and 20 cm of r, the lateral displacement from the electron beam axis. The absolute values of the measured activations are in good agreement with those calculated from the product of the $^{27}Al(n, \alpha)$ cross section[25] and $\psi_n(E_n, r, z)$ in Eq. (5), when r is equal to 10 cm and z is within about 5 cm, but the former becomes larger than the latter as r and z become large. This is because this approximate calculation neglects the electron-photon cascade and the photon scattering, so the neutron source distribution indicates a more pronounced forward peak than in fact. In spite of the rough approximation, this calculating

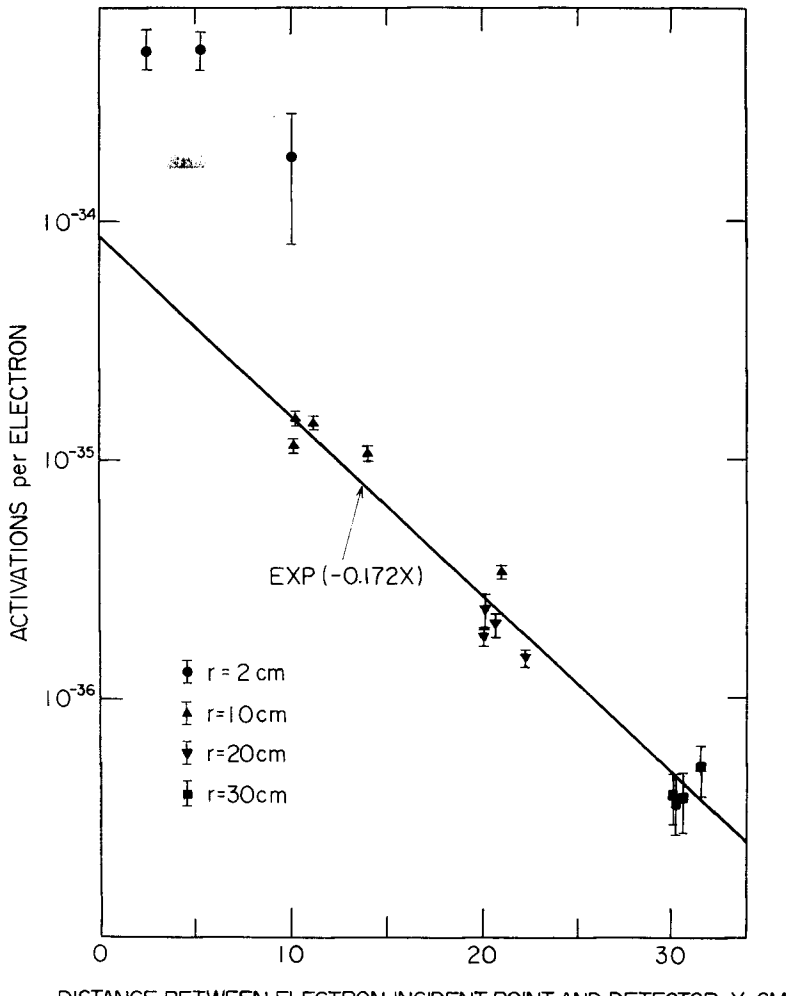

Fig. 7. Variation of the activations of aluminum detector with the distance betweenth the electron incident point and the detector position, $x=\sqrt{r^2+z^2}$.

method can account for the experimental results within the error of a factor of 2 when r and z are smaller than 20 and 10 cm, respectively.

The measured activations of the magnesium detector were compared with the aluminum ones. Fig. 6 shows that the effect of the $^{25}Mg(\gamma, p)^{24}Na$ reaction is remarkable when r is equal to 10 cm and z is between 2 and 5 cm.

The spacial distribution of neutron flux above about 6.5 MeV in the iron slab was obtained from the measured activations of the aluminum detectors. In Fig. 7, the activations are shown as a function of $x=\sqrt{r^2+z^2}$, the distance between the electron incident point and the detector position. These figures clearly show that for the aluminum detector, the activation rate decreases in exponential $e^{-\alpha x}$ excluding the vicinity of electron incident point, and α is very close to the effective removal cross section of iron ($\Sigma_{eff}{}^R=0.172$ cm^{-1})[26]. From this fact, it is concluded that the spacial distribution of neutrons is nearly spherical symmetric around the beam incident point and attenuates in the form of

$$\Phi(x) = \Phi(0)e^{-\Sigma_{eff}{}^R x}, \tag{8}$$

where x exceeds about 10 cm.

Acknowledgment

The authors wish to thank to Messrs. Y. Fujita and T. Matsumoto for their helpful contribution during the experiment at the Research Reactor Institute of Kyoto University.

References

1) A. R. Smith: UCRL-16323 (1965).
2) H. Hirayama, and T. Nakamura: Nucl. Sci. Eng., 50, 248 (1973).
3) T. Nakamura and H. Hirayama: At. Energy Soc. Japan, (in Japanese), 14 [12], 668 (1972).
4) C. D. Zerby and H. S. Moran: J. Appl. Phys., 34, 2445 (1963).
5) M. L. Berger and S. M. Seltzer: "Protection against Space Radiation", NASA SP-169, p. 285 (1968), National Aeronautics and Space Administration, Oak Ridge.
6) H. Sugiyama: Researches of the Electrotechnical Laboratory, (in Japanese), No. 724 (1972).
7) W. W. Scott: in Ref. (5), p. 339.
8) H. Ferdinande, G. Knuyt, R. Van de Vijver and R. Jacobs: Nucl. Instr. Methods, 91, 135 (1971).
9) T. Nakamura, M. Takemura, H. Hirayama and T. Hyodo: J. Appl. Phys., 43, 5189 (1972).
10) D. C. Irving, R. M. Jr. Freestone and F. B. K. Kam: ORNL-3622, (1965).
11) H. Hirayama and T. Nakamura: Mem. Facl. Eng., Kyoto Univ., 34 [2], 187 (1972).
12) S. Preiser, G. Rabinowitz and E. De Dufor: ARL Technical Report 60-314, (1960).
13) B. G. Carlson: LA-2996, (1964).
14) W. W. Jr. Engle: K-1693, (1967).

15) F. R. Mynatt: K-1694, (1968).
16) K. Takeuchi: J. Nucl. Sci. Technol., 8, 141 (1971).
17) W. C. Barber, and W. D. George: Phys. Rev., 116, 1551 (1959).
18) E. G. Fuller, et al.: "Shielding for High-Energy Electron Accelerator Installations", Natl. Bur. Stands. Handbook 97, (1964), U. S. Government Printing Office, Washington, D. C.
19) R. G. Jr. Alsmiller, T. A. Gabriel, and M. P. Guthrie: Nucl. Sci. Eng. 40, 365 (1970).
20) T. Nakamura: Nucl. Instr. Methods, 105, 77 (1972).
21) P. J. Ebert, A. F. Lauzon and E. M. Lent: Phys. Rev., 183, 422 (1969).
22) H. A. Bethe: Phys. Rev., 89, 1256 (1953).
23) V. H. Frank: Z. Naturforsch., A14, 247 (1959).
24) R. Montalbetti, L. Katz and J. Goldemberg: Phys. Rev., 91, 659 (1953).
25) A. M. Bresesti, M. Bresesti, A. Rota and R. A. Rydin: Nucl. Sci. Eng., 40, 331 (1970).
26) T. Nakamura, T. Kanazawa, Y. Hayashi and T. Hyodo: J. Nucl. Sci. Technol., 8, 481 (1971).